Driver-identified supervisory control system of hybrid electric vehicles based on spectrum-guided fuzzy feature extraction

Li, Ji; Zhou, Quan; He, Yinglong; Williams, Huw; Xu, Hongming

DOI:
10.1109/TFUZZ.2020.2972843

License:
Other (please specify with Rights Statement)

Document Version
Peer reviewed version

Citation for published version (Harvard):
Li, J, Zhou, Q, He, Y, Williams, H & Xu, H 2020, 'Driver-identified supervisory control system of hybrid electric vehicles based on spectrum-guided fuzzy feature extraction', *IEEE Transactions on Fuzzy Systems*, vol. 28, no. 11, 8993840, pp. 2691-2701. https://doi.org/10.1109/TFUZZ.2020.2972843

Driver-identified Supervisory Control System of Hybrid Electric Vehicles based on Spectrum-guided Fuzzy Feature Extraction

Ji Li, *Member, IEEE*, Quan Zhou, *Member, IEEE*, Yinglong He, Huw Williams, and Hongming Xu*

***Abstract*—This paper introduces the concept of the driver-identified supervisory control system, which forms a novel architecture of adaptive energy management for hybrid electric vehicles (HEVs). As a man-machine system, the proposed system can accurately identify the human driver from natural operating signals and provides driver-identified globally optimal control policies as opposed to mere control actions. To help improve the identifiability and efficiency of this control system, the method of spectrum-guided fuzzy feature extraction (SFFE) is developed. Firstly, the configuration of the HEV model and its control system are analyzed. Secondly, design procedures of the SFFE algorithm are set out to extract 15 groups of features from primitive operating signals. Thirdly, long-term and short-term memory networks are developed as a driver recognizer and tested by the features. The driver identity maps to corresponding control policies optimized by dynamic programming. Finally, the comparative study includes involved extraction methods and their identification system performance as well as their application to HEV systems. The results demonstrate that with help of the SFFE, the driver recognizer improves identifiability by at least 10% compared to that obtained using other involved extraction methods. The improved HEV system is a significant advance over the 5.53% reduction on fuel consumption obtained by the fuzzy-logic-based system.**

***Index Terms*—Adaptive supervisory control; deep recurrent LSTM network; driver identification; dynamic programming; feature extraction; hybrid electric vehicles**

I. Introduction

PERSISTENT environmental issues and periodic energy crises are major concerns for the automobile industry [1]. As an emerging trend, vehicle electrification aims to investigate alternative powertrain technologies and offer potentially fuel-efficient solutions in propulsion systems, traffic strategies and urban studies [2]. Hybrid technology is a good transition solution to environmental pollution that makes it possible to both improve the fuel economy and reduce the exhaust emissions of vehicles [3], [4]. For hybrid electric vehicles (HEVs), developing optimal energy management strategies is critical to achieving the best performance and energy efficiency through power-split control. As another primary element, the driver plays a significant role in safety and eco-driving [5]. Most of the literature currently ignores the human driver error in eco-driving, leading to errors in tracking the recommended velocity profiles. In reality, the driver may not follow the optimal velocity precisely and this uncertainty may affect the velocity tracking performance and increase fuel consumption [6]. Thus, vehicle control strategies that seek highly optimized performance need to optimize the system composed of both the vehicle and the driver.

Classical control strategies have difficulty in meeting the requirements of this standard, because the driver's information is not easy to exploit in real time [7]. In order to break through this bottleneck, scholars and industry started to shift their focus to forward information fusion in supervisory control systems (i.e. driving-feature-related identification and prediction) [8]. This scheme deepens the consideration of individual driving style and incorporates this factor into the decision-making of energy allocation in HEV systems [9]. It makes smart cars operate in a more human-like way to explore control strategies that are more efficient rather than following a standardized strategy. In this case, this paper classifies the state-of-the-art of energy management strategies into two aspects based on whether the driver behavior related is involved or not and discuss them as follows.

Modelling driving behavior in the HEV energy management requires accurate quantification of the relationship between driving behavior and fuel consumption [10]. Li et al. employ K-means to classify driving behaviors with rigid boundaries but the uncertainty of driving behavior is not considered [11]. Wahab et al. use Gaussian mixture models (GMMs) to extract driving feature, training by fuzzy neural networks [12]. However, the applicability of GMMs to other environments is debatable. Xie et al. integrate Markov chain (MC) models and dynamic programming (DP) to implement stochastic model predictive control for plug-in hybrid electric buses [13]. In fact, some dramatic driving states may be homogenized into a very low probability distribution or even ignored altogether in the training process of a MC model. This issue may occur in the work of Cairano et al. [14]. Zhang et al. construct a hierarchical driving behavior model, providing in-depth knowledge about behavior generation, transmission, and consequence [15], but the rationality of its classification needs to be further explored and its simulation results should be validated in real

The authors are with the Department of Mechanical Engineering, the University of Birmingham, Birmingham B15 2TT, U.K. (e-mail: jxl592@bham.ac.uk; q.zhou@pgr.bham.ac.uk; yxh701@bham.ac.uk; huw.trefor.williams@gmail.com; h.m.xu@bham.ac.uk).

applications. Lei et al. utilize a sliding window driving pattern search algorithm which incorporates offline particle swarm optimization [16], but the algorithm is flawed and fails to find global optimal solutions [17]. Li et al. create an online velocity predictor, and it helps guarantee the effectiveness of swarm-based optimal control sequences in energy-saving [18]. Similar to the work of Zhang et al. [19], most of the existing research on the division of driver behavior is 'driving-style-based'. Such hierarchical driver models, however, result in the consequence that the control policy optimized for a single style may lose the global optimal advantage during mode switching.

There is also a considerable amount of literature concerned with supervisory control systems that introduce emerging technologies and methodologies. Kolmanovsky et al. describe the development and experimental implementation of game theory for HEV energy management [20]. Game theory, however, requires deep knowledge of the system elements and consequently cannot be extrapolated to other vehicle types [21]. Zhou et al. research a 'model-free' predictive energy management system for increasing the prediction horizon length by 71% from model-based one [22]. Deep reinforcement learning [23], has been employed by Wu et al. to develop a continuous control strategy for hybrid electric buses [24]. But the feasibility and stability of implementing such model-free algorithms into an actual vehicle controller needs to be further investigated and validated. Sorrentino et al. develop flexible procedures for co-optimizing design and control of fuel cell hybrid vehicles and its outcomes yield useful guidelines that support decision making in the design process [25]. In the work of Ahmadi et al., a genetic algorithm is invoked to accurately adjust control parameters of an FLC, and its results show that fuel economy and vehicle performance are significantly improved [26]. In the work of Kheirandish et al., a dynamic fuzzy cognitive network is proposed to describe the behavior of a fuel cell electric bicycle system [27]. Moreover, some other type of fuzzy-logic-based control system are employed for HEV energy management such as neuro-fuzzy [28], genetic-fuzzy [29] and Takagi-Sugeno fuzzy [30] control systems. However, such fuzzy-logic-based supervisory control systems are established based on human cognition and their performances are largely limited by empirical knowledge.

In order to break through the limitations of the aforementioned research, this paper proposes the novel adaptive energy management architecture of a driver-identified supervisory control system. Differing from conventional adaptive control systems with driving-style-based adjustment, the proposed system can accurately identify the human driver from natural operating signals and provides driver-identified globally optimal control policies as opposed to mere control actions. To help improve identifiability and efficiency of this control system, the method of spectrum-guided fuzzy feature extraction (SFFE) is developed to exploit spectral information after defuzzification integration for adaptively adjusting the size of the sampling window. Firstly, the configuration of the HEV model is analyzed and its control-oriented optimization problem is formulated. Secondly, the structure of the driver-identified supervisory control system is presented, and design procedures of the SFFE algorithm are set out beginning with conventional methods to extract 15 groups of features from primitive operating signals. Thirdly, long short-term memory (LSTM) networks are developed as a driver recognizer and tested by the aforementioned features. The driver identity is then mapped to corresponding control policies optimized by dynamic programming. Finally, the comparative study includes involved extraction methods and their identification system performance as well as their application to HEV systems.

Following the introduction, the configuration of the HEV and its control-oriented optimization problem are analyzed in section II. Section III elaborates the structure of the driver-identified supervisory control system and the design procedures of the SFFE algorithm, followed by recognizer training and controller optimization of the HEV system. Section IV declares the collection process of testing cycles, the human driver who created it as well as the driving simulation platform used. Section V investigates the comparative study of involved extraction methods and their identification system performance as well as their application to HEV systems. Conclusions are summarized in section VI.

II. Vehicle Configuration and Problem Formulation

A. HEV Configuration

The series-parallel HEV powertrain supervised by the vehicle controller, includes one gasoline engine, one integrated starter-generator (ISG), one trans-motor and two energy sources of fuel and electricity as shown in Fig. 1. In this case, the powers from the ICE after the transmission and the trans-motor are combined by coupling their speeds, where the speeds of the two power plants are decoupled to be chosen freely as described in [31]. The peak power of the trans-motor is $P_{mot^*} = 75$ kW (kilowatt) with 270 N · m (newton - meter) peak torque. The peak power of the gasoline engine is $P_{ICE^*} = 63$ kW with 140 N · m peak torque. The peak power of the ISG is $P_{ISG^*} = 32$ kW. The data for all of the components is provided by the ADVISOR software. Their suitability has been established in the authors' previous work [18], [32]. The authors are committed to continuing development of the control system using the same vehicle model for driveline system analysis and optimization. The main parameters of the HEV model are shown in Table I.

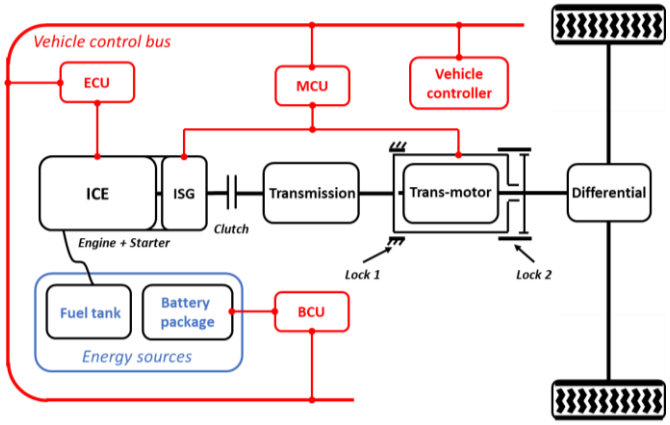

Fig. 1. The structure of the series-parallel HEV powertrain

TABLE I
MAIN PARAMETERS OF THE HEV MODEL

Symbol	Parameters	Values
M	Gross mass	1,500 kg
A_f	Windward area	2 m^2
R_{wh}	Tire rolling radius	0.3 m
C_d	Air drag coefficient	0.3
i_0	Differential ratio	3.75
i_g	Transmission ratio	3.55/1.96/1.30/0.89/0.71

B. Problem Formulation

In order to rationally assign the demand power of the powertrain to different power sources, the demand power of the powertrain and the state of charge (SoC) value of the battery package (BP) are treated as two input variables and the two output variables are the rotational speed of traction motor and the required power of the ISG. Here, the supervisory control system comprises two modes of pure electric traction and optimization-based traction, which can be expressed as

$$(T_{mot}, n_{mot}, P_{ice}, P_{gen}) = \begin{cases} Mode_{EV}(P_d, SoC), 0.8 \geq SoC > 0.5 \\ Mode_{opt.}(P_d, SoC), 0.5 \geq SoC > 0.2 \end{cases} \quad (1)$$

where, $Mode_{EV}$ indicates a pure electric traction mode; $Mode_{opt.}$ indicates an optimization-based control mode; T_{mot} is the torque of traction motor; n_{mot} is the rotational speed of traction motor; P_{ice} is the power of internal combustion engine; P_{gen} is the power of the integrated starter-generator; P_d is the demand power of the powertrain; and SoC is the BP's state of charge. To ensure the BP is performing under proper conditions and to protect the BP from over discharge and over charge, the battery's SoC should remain in the range, $0.2 < SoC \leq 0.8$ as recommended [33].

In the electric traction mode, enough battery current can be supplied to satisfy the powertrain demand independently so that neither the ICE nor the ISG need to operate. The power distribution in this state is

$$\left.\begin{array}{c} T_{mot,k} = T_{d,k} \\ n_{mot,k} = \dfrac{P_{d,k}}{T_{mot,k}} \cdot 9550 \\ P_{gen,k} = 0 \\ P_{ICE,k} = 0 \end{array}\right\}, \quad (2)$$

where the constant 9550 is a conversion factor when units of torque, power and rotation speed are newton - meter, kilowatt, and revolutions per minute, respectively. The optimization-based control mode allows ICE power to be used either to simultaneously drive the vehicle and charge the BP or to partially drive the vehicle supplemented by a BP-charge-depleting drive from the trans-motor, depending on the sign of the trans-motor speed, n_{mot} (negative charges, positive depletes). The power distribution in this state is therefore given by

$$\left.\begin{array}{c} T_{mot,k} = T_{d,k} \\ n_{mot,k} = n_{mot\_opt,k} \\ P_{gen,k} = P_{gen\_opt,k} \\ P_{ICE,k} = -P_{gen,k} + \left(P_{d,k} - \dfrac{T_{mot,k} \cdot n_{mot,k}}{9550}\right) \end{array}\right\}, \quad (3)$$

where $n_{mot\_opt,k}$ is the optimal rotation speed of the traction motor; and $P_{gen\_opt,k}$ is the optimal demand power of the ISG. Based on Eq. (3), the state equation of the HEV model can be generally expressed in discrete-time format by the following equation

$$\left.\begin{array}{c} x_{k+1} = f(x_k, u_k) \\ x = SoC \\ u_k = [n_{mot\_opt,k} \quad P_{gen\_opt,k}] \end{array}\right\}, \quad (4)$$

where, x is the state variable; k is the integer-valued discrete time variable; and u denotes the control variable expressed as a vector of the optimized rotational speed n_{mot_opt} of the traction motor and the optimized demand power P_{gen_opt} of the ISG.

The principal optimization target for HEV systems is to reduce fossil fuel consumption by obtaining energy from the electricity grid. The following cost function for minimizing fuel consumption will be adopted

$$\min J = \sum_{k=0}^{N-1} L(x_k, u_k) = \sum_{k=0}^{N-1} E_{fuel,k}, \quad (5)$$

where, N is the length of the driving cycle in discrete time-steps, L is the instantaneous cost, and E_{fuel} is the instantaneous fuel consumption at the kth time step. To ensure a smooth operation of engine, ISG, traction motor, and battery, the following constraints will be needed for the optimization.

$$s.t. \begin{cases} T_{mot,k}, & -T^*_{mot} \leq T_{mot,k} \leq T^*_{mot} \\ n_{mot\_opt,k}, & 0 \leq n_{mot\_opt,k} \leq n^*_{mot} \\ P_{ICE,k}, & 0 \leq P_{ICE,k} \leq P^*_{ICE} \\ P_{gen\_opt,k}, & -P_{ISG^*} \leq P_{gen\_opt,k} \leq 0 \\ SoC_k, & 0.2 < SoC_k \leq 0.8 \end{cases}, \quad (6)$$

where, T^*_{mot} and n^*_{mot} are the maximum torque and the maximum rotational speed of the traction motor; P^*_{ICE} and P_{ISG^*} are the maximum power of the engine and of ISG.

III. DRIVER-IDENTIFIED SUPERVISORY CONTROL SYSTEM

A. System Architecture

The proposed driver-identified supervisory control system includes one LSTM-based driver recognizer and one DP-based supervisory controller as shown in Fig. 2. During real-time driving, human drivers generate primitive operating signals which are collected by a driving simulator. Due to primitive operating signals with interference information redundancy, driving feature extraction is needed to improve the identifiability and the efficiency of this control system. Through feature extraction, these extracted signals will be used as inputs to the recognizer identifying drivers that each bridge to their own control policy in the supervisory controller. Finally, the driver-identified control signal will be sent to the HEV powertrain to manage energy utilization.

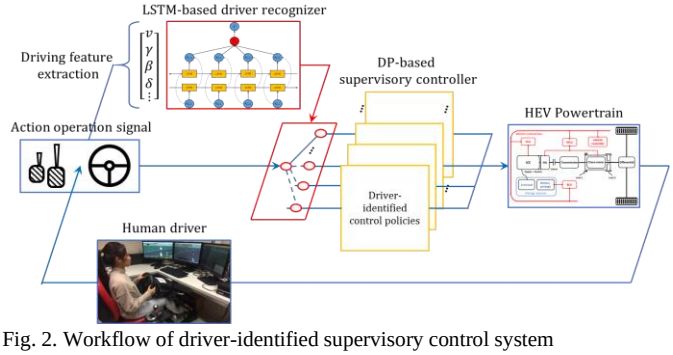

Fig. 2. Workflow of driver-identified supervisory control system

B. Driving Feature Extraction

To improve identifiability of the driver-identified supervisory control system, characterization of the training material is needed for the extraction of hidden features from the time-series of the primitive operating signals. The driving operating signals studied in this paper are vehicle speed, gas pedal deflection, brake pedal deflection, and steering angle. Compared to other signals that need to be detected with additional sensors, they were shown to be a pragmatic choice for driving style recognition by Martinez et al [9]. This section starts with the primitive operation signals namely Feature 0 and follows by introducing the rest of 14 groups of features that are respectively extracted by time-domain, frequency-domain and the proposed SFFE methods.

Feature 0: The driving operating signals originally collected from a driving simulator are regarded as the baseline in this research and are combined into the row vector, $[v \quad \gamma \quad \beta \quad \delta]$, where v is vehicle speed (km/h); γ is gas pedal deflection (%); β is brake pedal deflection (%); and δ is the steering angle (rad).

1) Time and Frequency Domain Extractions

In the widely used time-domain extraction technique, a short-term sliding window is introduced to standardize the sampling dimension and lengthen the memory time of characteristic states. Here, the dataset of driving operating signals is defined, in which each time step k of data is expressed as given by:

$$(\boldsymbol{v},\boldsymbol{\gamma},\boldsymbol{\beta},\boldsymbol{\delta})^T=\begin{bmatrix} v_{k-h+1} & v_{k-h+2} & \cdots & v_k \\ \gamma_{k-h+1} & \gamma_{k-h+2} & \cdots & \gamma_k \\ \beta_{k-h+1} & \beta_{k-h+2} & \cdots & \beta_k \\ \delta_{k-h+1} & \delta_{k-h+2} & \cdots & \delta_k \end{bmatrix} \tag{7}$$

where, h is length of the short-term sliding window, which is taken to be the discrete time equivalent of 60 seconds.

Feature 1: The maximum values of the four elements in the time-domain are adopted to reflect the operating intensity of drivers. Based on Eq. (7), their values can be calculated by

$$(v_{max},\gamma_{max},\beta_{max},\delta_{max})=\max(\boldsymbol{v},\boldsymbol{\gamma},\boldsymbol{\beta},\boldsymbol{\delta}_{abs})^T \ , \tag{8}$$

where $\boldsymbol{\delta}_{abs}$ denotes the element wise absolute value of $\boldsymbol{\delta}$.

Feature 2: The maximum ranges of the four elements in the time-domain are adopted to reflect the operating proficiency of drivers. In general, drivers with higher operating proficiency have lower maximum range. Based on Eq. (7), their values can be calculated by

$$\begin{aligned}&(v_{rng.},\gamma_{rng.},\beta_{rng.},\delta_{rng.})\\&\quad=\max(\boldsymbol{v},\boldsymbol{\gamma},\boldsymbol{\beta},\boldsymbol{\delta}_{abs})^T-\min(\boldsymbol{v},\boldsymbol{\gamma},\boldsymbol{\beta},\boldsymbol{\delta}_{abs})^T \ .\end{aligned} \tag{9}$$

Feature 3: The average values of the four elements in the time-domain are adopted to reflect driving habits. The authors hypothesize that this factor is related to the driving geography and the environment but a discussion of this hypothesis is beyond the scope of this paper and will be left as a topic for future research. Based on Eq. (7), the average values of the four elements in the time-domain are

$$(v_{avg.},\gamma_{avg.},\beta_{avg.},\delta_{avg.})=\frac{\sum_{i=0}^{i=h}(\boldsymbol{v},\boldsymbol{\gamma},\boldsymbol{\beta},\boldsymbol{\delta}_{abs})^T}{h} \ . \tag{10}$$

Another mainstream extraction method to determine the extent of pre-processing human behaviors is frequency domain extraction [34]. Here, the discrete (fast) Fourier transform (DFT) is used to calculate three principal features and they will be examined later when training the recognizer. Therefore, the DFT of matrix Eq. (7) can be written

$$(\boldsymbol{H}_v,\boldsymbol{H}_\gamma,\boldsymbol{H}_\beta,\boldsymbol{H}_\delta)^T=\begin{bmatrix} H_{v,1} & H_{v,2} & \cdots & H_{v,L} \\ H_{\gamma,1} & H_{\gamma,2} & \cdots & H_{\gamma,L} \\ H_{\beta,1} & H_{\beta,2} & \cdots & H_{\beta,L} \\ H_{\delta,1} & H_{\delta,2} & \cdots & H_{\delta,L} \end{bmatrix} \tag{11}$$

where, $H_v, H_\gamma, H_\beta, H_\delta$ denote the single-sided amplitude spectra corresponding to vehicle speed, gas pedal deflection, brake pedal deflection, and steering angle, respectively; and $L=h/2$.

Feature 4: The maximum magnitudes of the four elements in the frequency domain are used to express the spectral intensity of driving operation via the equation,

$$\begin{aligned}&(H_{v\_max,k},H_{\gamma\_max,k},H_{\beta\_max,k},H_{\delta\_max,k})\\&\quad=\max(\boldsymbol{H}_v,\boldsymbol{H}_\gamma,\boldsymbol{H}_\beta,\boldsymbol{H}_\delta)^T \ ,\end{aligned} \tag{12}$$

Feature 5: The frequencies corresponding to the maximum magnitudes (denoted by $\max freq$) of the four elements in the frequency domain are used to express the regularity of driving operation via the equation,

$$\begin{aligned}&(f^*_{v\_max,k},f^*_{\varrho\_max,k},f^*_{\sigma\_max,k},f^*_{\varsigma\_max,k})\\&\quad=\max freq(\boldsymbol{H}_v,\boldsymbol{H}_\gamma,\boldsymbol{H}_\beta,\boldsymbol{H}_\delta)^T \ .\end{aligned} \tag{13}$$

Feature 6: As another feature to express the regularity of driving operation, the frequencies corresponding to the centroids of the four elements in the frequency domain are considered. They are defined as follows:

$$\begin{aligned}&(H^*_{v\_cen,k},H^*_{\varrho\_cen,k},H^*_{\sigma\_cen,k},H^*_{\varsigma\_cen,k})\\&\quad=\frac{\sum_{i=1}^{i=L}f_i\times(H_{v,i},H_{\gamma,i},H_{\beta,i},H_{\delta,i})}{\sum_{i=1}^{i=L}f_i} \ ,\end{aligned} \tag{14}$$

in which

$$f_i=\frac{Fs}{h}i, \qquad i=1,2,\dots,L, \tag{15}$$

where, $Fs=1000$ Hz is the sampling frequency.

2) Spectrum-guided Fuzzy Feature Extraction

It should be noted that instantaneous changes in driver behavior might affect the characteristic expression of the time-series data during real-time driving. The SFFE activates the sampling window and uses frequency-domain characteristics as the basis for adaptively adjusting the window size. It is developed to ensure the classification accuracy while adaptively searching for a more appropriate minimum size of the sliding window. Ideally, it can enable the elimination of the effects of sudden driver behavior changes on the characteristic expression of the time-series data through adaptively adjusting the size of the short-term sliding window. The consideration of spectral features easily captures essential attributes from the dynamic driving signals and they can be exploited as an important factor in adjusting window size. Inspired by fuzzy encoding technology, all spectral features are integrated to balance the contribution of each element to the window size, thereby guiding time-domain extraction. The design procedures of the SFFE are:

Feature 7-15: The fuzzy sets with linguistic terms are regulated with standard triangular membership functions (MFs), where the degree of membership is expressed as a function of normalized values in the interval, [0,1]. The values of the MFs

in the FLC are set at three levels: Low, Medium, and High. These functions fuzzify the crisp inputs. Here, the inputs of the FLC need to be sensitively scaled to maintain the boundaries of their working area. They are formulated mathematically through the relationship,

$$(v^*, \gamma^*, \beta^*, \delta^*) = \left(\frac{v_f - v_f^-}{v_f^+ - v_f^-}, \frac{\gamma_f - \gamma_f^-}{\gamma_f^+ - \gamma_f^-}, \frac{\beta_f - \beta_f^-}{\beta_f^+ - \beta_f^-}, \frac{\delta_f - \delta_f^-}{\delta_f^+ - \delta_f^-}\right), \quad (16)$$

where, $v_f, \gamma_f, \beta_f, \delta_f$ indicate spectral feature signals related to speed, gas, brake and steering angle; $\cdot^-$ and $\cdot^+$ indicate the corresponding minimum and maximum; and $\cdot^*$ indicates the corresponding scaled input, $[0,1]$. The rule base determines the control output O with the inputs states A, B, C, and D by applying a 'if A and B and C and D then O' policy. A mathematical expression of the 'if A and B and C and D then O' policy is

$$O = (A \times B \times C \times D) \circ R\,. \quad (17)$$

where, 'A', 'B', 'C', 'D' denote the fuzzy sets of scaled spectral signals related to speed, gas, brake and steering angle; 'O' denotes the crisp of the reference of scalar coefficient $[0,1]$ for the size of sliding windows; and 'R' denotes the fuzzy relation matrix by cross-product of four fuzzy sets of inputs.

To simplify the expression of $3^4 = 81$ fuzzy logic inferences, we assign values to linguistic sets: 'Short' $= 1$; 'Medium' $= 2$; 'Long' $= 3$. Therefore, the reasoning process that is based on Eq. (17) with the Sugeno fuzzy set can then be described by the following if-then statements:

$$\left.\begin{array}{c}\text{if } A+B+C+D \in [4,6]\\ \text{if } A+B+C+D \in [7,9]\\ \text{if } A+B+C+D \in [10,12]\end{array}\right\} \text{ then O is } \begin{cases}\text{Long}\\ \text{Medium}\\ \text{Short}\end{cases} \quad (18)$$

In this inference mechanism, the implied fuzzy sets are produced using the max–min composition. In defuzzification, these implied fuzzy sets are combined to provide a crisp value of the controller outputs. There are several approaches [35] to accomplish the defuzzification process, of which the centroid of area method has been chosen for this case. The final output is then measured as the average of the individual centroids weighted by their membership values as follows:

$$\left.\begin{array}{c} O = \dfrac{\sum_{i=1}^{n} Out_i \cdot \varphi_i}{\sum_{i=1}^{n} \varphi_i} \\ h^* = h - \dfrac{h}{2} O \end{array}\right\}, \quad (19)$$

where, Out_i is the output of rule base i; φ_i is the centre of the output MF; and h^* is the size of the adaptive sliding window. In this paper, these functions are taken as a triangular membership function as follows:

$$q_i = \max\left(\min\left(\frac{x - (0.5i - 0.9)}{0.4}, \frac{(0.5i - 0.1) - x}{0.4}\right), 0\right), \quad i = 1,2,3. \quad (20)$$

Through fuzzy encoding technology, the proposed method extracts 3×3 permutations between time and frequency domain. i.e. nine groups of extra features. Their mapping relation is expressed as shown in Fig. 3. As an upgraded version of time-domain extraction, the purpose is the elimination of the effects of sudden driver behavior changes on the characteristic expression of the time-series data. So far, 15 groups of features extracted from the original operating signals are obtained and then used as training data for the driver recognizer. These will be discussed in the next section.

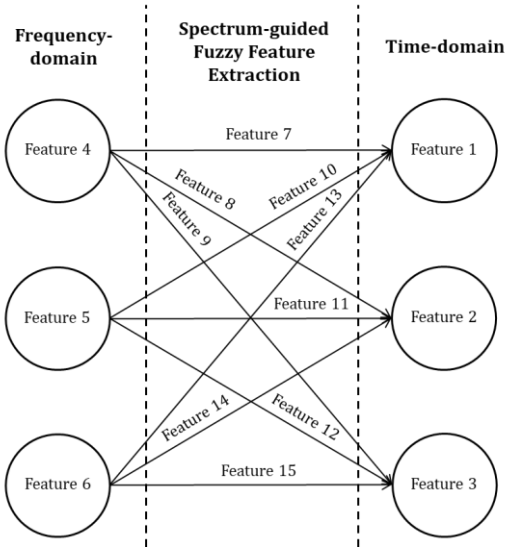

Fig. 3. Mapping relation in spectrum-guided fuzzy feature extraction

C. Recognizer Training and Controller Optimization

This section introduces two principal parts to develop the driver-identified supervisory control system: 1) the structure and training data of networks to be trained; 2) the driver-identified dynamic programming for controller optimization.

1) Bidirectional LSTMs and training data

To efficiently classify each time step of the extracted sequence data, a bidirectional recurrent neural network (RNN) is adopted as a model that can overcome various restrictions inherent in conventional RNNs. This model divides regular RNN neuron states into forward and backward. These two networks connect to the same output layer to generate output information. With this structure, both past and future situations of sequential inputs in a time frame are evaluated without delay [36]. After 20 runs of the repeatability test for 10, 20, 50, 100, and 200 one-cell memory blocks, using 100 one-cell memory blocks achieved the highest value of average identifiability. Thus, a Bi-directional LSTM network, with two hidden LSTM layers, both containing 100 one-cell memory blocks of one cell each is used in this research.

To gain a better understanding of the contribution of each feature to driver identification, ablation studies are performed to divide the training data and the extracted features into two categories for each extraction method: one category is target features; the remaining category is non-target features. In each ablation, one feature is removed from all combinations of single types. E.g. in time-domain extraction methods, if Feature 1 is regarded as a target feature, Features 2 and 3 are the corresponding non-target features. If Feature 2 is regarded as the target feature, Features 1 and 3 are the corresponding non-target features. Similar arguments can be applied in other cases.

2) Driver-identified dynamic programming

According to the decision of the LSTM-based driver recognizer, the control policies in the DP-based control mode

need to be adaptively switched for each driver. Therefore, the control variables must be redetermined and their definition is

$$u_k = \Phi_i(SoC_k), \tag{21}$$

in which

$$i = \mathbb{Z}_{lstm}(v_k, \gamma_k, \beta_k, \delta_k), i = [A, B, C, D, \dots], \tag{22}$$

where u is the control variable; Φ_i is the DP-based control policy for index i driver; and $\mathbb{Z}_{lstm}$ is the LSTM-based network to determine the driver behavior.

In the optimization-based control mode, DP is employed to locate the optimized control actions at each stage by minimizing the fuel consumption cost function over a certain driving cycle. As an industry-recognized global optimization algorithm, DP can efficiently handle the constraints and nonlinearity of a problem and find a global optimal solution [37]. Here, the DP problem is described as the recursive Eqs. (23) and (24), which can be solved through backward recursion. The sub-problem for the $(N_i - 1)$th step is

$$J^*_{N_i-1}(x_{N_i-1}) = \min_{u_{N_i-1}} \left[L(x_{N_i-1}, u_{N_i-1}) + G(x_{N_i})\right]. \tag{23}$$

For the kth $0 \le k < N_i - 1$ step, the sub-problem is given by

$$J^*_k(x_k) = \min_{u_k}[L(x_k, u_k) + G(x_k)] \quad , \tag{24}$$

where, $J^*_k(x_k)$ is the optimal cost-to-go function at state x_k from the kth step to the termination of the driving cycle, and x_{k+1} is the state in the $(k+1)$th step after the control variable u_k is applied to state x_k at the kth step according to Eq. (24).

IV. Experimental Set-up

A. Data Collection in Driver Simulator

In this paper, data collection is conducted on the cockpit package (supported by a Thrustmaster T500RS) with the same HEV model with an automatic gearbox as Fig. 4. This is to make sure the driving characteristics exhibited by them are under the same constraints and their results are comparable. With respect to real-world road conditions, the road map model used with reconstructed traffic simulates a cyclic undivided highway with uphill, downhill, curved and straight roads and is provided by IPG CarMaker. To reduce the impact of differing traffic and road conditions on human drivers, they are restricted to the same cycling road conditions and required to follow the speed limits, stop signs, traffic lights, and other traffic regulations. It should be noted that the driver's pedal behavior might be dependent on the vehicle, the pedal to torque map, and even the physical pedal resistance feedback.

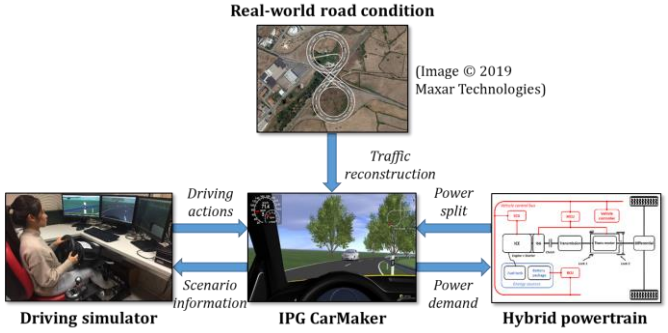

Fig. 4. Collection process of driving profiles

B. Driving Operation Patterns

Observable driving signals can be categorized into three groups [34]: 1) driving behavior, e.g., gas and brake pedal pressures and steering angles; 2) vehicle status, e.g., velocity, acceleration, and engine speed; and 3) vehicle position, e.g., following distance, relative lane position, and yaw angle. Among these driving signals, we focus on driving behavior with respect to the relationship between velocity, gas, brake pedal, and steering angle operating signals. Table 2 organizes driving-related information about six subjects.

TABLE II
DRIVING INFORMATION OF SIX SUBJECTS

Driver	Age	Time to hold a driving license (yrs.)	Annual mileage (mile)	Driving geography
A	27	10	2000	Urban
B	27	5	3000	Hybrid
C	24	7	2500	Hybrid
D	26	10	1500	Hybrid
E	26	4	6000	Motorway
F	30	1	1000	Urban

Fig. 5 shows driving operation pattern examples of 10-min driving signals collected in the simulator with a 10Hz sampling frequency, wherein (a) is used for training and (b) is used for testing and their data capacity ratio is 5:6. For one single driver, 6000×4 original signal data has been collected. Data from Driver F is only used as testing data to further validate the system robustness. It can be seen that primitive driving operation patterns are like a 'yarn ball' and their fragments are intertwined. It is difficult to distinguish their owners under the same road conditions.

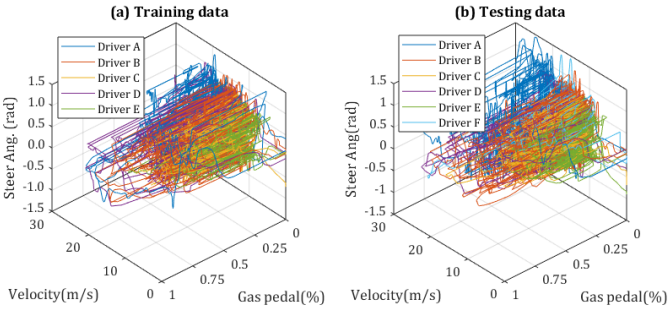

Fig. 5. Driving profiles during designed road condition

V. Results and Discussions

A. Significant Difference Analysis

In this section, the significant difference of extraction results are analyzed and the Mann-Whiney U test is conducted to determine whether two independent driver samples were selected from populations having the same distribution without the assumption of normal distributions. Fig. 6 shows p-value results based on the null hypothesis of no significant difference between the two drivers of primitive operation data, in which p-values greater than 0.05 are marked in red. From the results, the primitive velocity samples between every two drivers all have a statistical difference, while some groups of the rest of the primitive samples between every two drivers have no statistically significant difference. Especially for primitive steering angle samples, the distribution differences for each pair of drivers is hard to statistically distinguish.

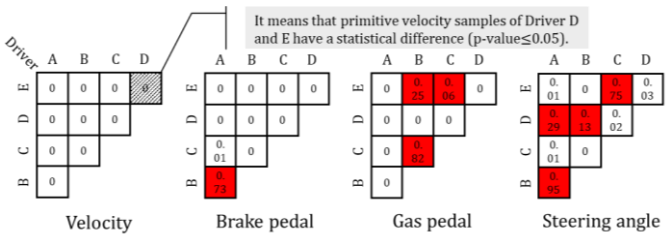

Fig. 6. Mann-Whiney U test results of original driving profile

Based on the results of Mann-Whiney U test, the independence factor is chosen to represent the performance of the original data by using all extraction methods. The extraction method with a higher independence factor provides better performance in terms of the significant difference results. Its definition is

$$I_i = \frac{Num_{\leq 0.05}}{Num_{all}} \quad , \tag{25}$$

where, $Num_{\leq 0.05}$ is the number of p-values less than or equal to 0.05 of significant differences between each pair of drivers; Num_{all} is the number of all trials. Calculating by Eq. (25), the independence factor values of all involved extraction methods are presented in Table II.

TABLE II
INDEPENDENCE FACTOR OF USING INVOLVED EXTRACTION METHODS

	Original	Time	Frequency	SFFE-4	SFFE-5	SFFE-6
$Num_{\leq 0.05}$	32	118	113	120	120	120
Num_{all}	40	120	120	120	120	120
I_i	0.80	0.98	0.94	1.00	1.00	1.00

Notes: the SFFE-4, -5, and -6 denote using the Feature 4, 5, and 6 as different spectral signals to guide extraction respectively.

By comparing the independence factor value, all extraction methods have a certain degree of improvement in stripping the driver's characteristics from the original driving data. Compared to time or frequency domain methods, the proposed SFFE can be more robustly implemented for these test drivers following the same road scenario. Through adaptively adjusting the size of sampling windows, this method can capture driving characteristics more accurately under relatively harsh conditions. Moreover, the types of features collected may limit their significant difference. To evaluate the contribution of existing driving characteristics to driver identifiability is another interesting and independent topic that could be studied in future work.

B. Identification Performance Comparison

In Table III, the contribution of the extracted feature (training material) types to driver identification is investigated. An initial experiment was conducted on every single feature of using different extraction methods (Target groups). As [38] considered, the ablation validation was performed for features other than selected single features (Non-target groups). The training process, which uses each feature extracted from the training cycles, has been repeated 20 times and the best testing results for each feature and network structures is recorded respectively. After investigation, the training parameters of the networks were set at 100 hidden units, 0.01 initial learn rate and 80 maximum epochs that are convergent and efficient.

It is seen that all three methods have a certain improvement in the characterization of the original data (59.2%), in which SFFE-5 method realize the highest identifiability of 96.1% by using Bi-LSTM networks without Feature 2. The method proposed by Wijnands et al. uses non-extracted data for training purposes so it is clearly not applicable in this case [39]. From the perspective of extraction methods, the proposed SFFE ranks first with the 80.4% average identifiability compared to those of time domain (71.9%) and frequency domain (68.0%) extraction methods. From the perspective of network structure, the Bi-LSTM network has 78.6% average identifiability and the forward one has 71.7% average identifiability. With the double feature dimensions of training, the identifiability generally has an upward trend (average 9.35% up), whereas it does not work for the original data.

Figure 8 shows real-time driver identification that compares the best performance of each type of extraction methods, which includes the original (Feature 0), time-domain (Feature 3), frequency-domain (Feature 5) and the proposed SFFE (Feature 11). During real-time driving, the original data driven driver recognizer cannot identify the driver from their driving operation signal. Training by using time domain or frequency domain data improves the recognition accuracy of the driver

TABLE III
IDENTIFIABILITY COMPARISON FROM VIEW OF FEATURES AND NETWORKS

Feature		Forward LSTM		Bidirectional LSTM		Average identifiability	
Type	Num.	Target	Non-target	Target	Non-target	Each num.	Each type
Original	0	0.590	0.590	0.593	0.593	0.592	0.592
Time-domain	1	0.579	0.653	0.749	0.726	0.677	
	2	0.599	0.714	0.622	0.833	0.692	0.719
	3	0.76	0.655	0.836	0.800	0.788	
Frequency-domain	4	0.604	0.514	0.651	0.804	0.643	
	5	0.621	0.645	0.618	0.829	0.678	0.680
	6	0.565	0.764	0.785	0.754	0.717	
SFFE-4	7	0.745	0.758	0.773	0.806	0.771	
	8	0.776	0.906	0.733	0.909	0.806	0.798
	9	0.796	0.749	0.756	0.863	0.766	
SFFE-5	10	0.798	0.793	0.906	0.861	0.840	
	11	0.835	0.870	0.939	0.961	0.8940	0.855
	12	0.723	0.817	0.878	0.920	0.825	
SFFE-6	13	0.763	0.765	0.818	0.891	0.809	
	14	0.783	0.838	0.738	0.853	0.778	0.803
	15	0.761	0.721	0.797	0.914	0.748	
Average identifiability		0.706	0.762	0.735	0.832	0.759	

recognizer, especially for Drivers A, D, and E. Training by using data extracted by the proposed SFFE can further improve recognition accuracy of Driver C and reduce the size of sampling windows from 60 s to 47 s, but there still is a defect in identifying Driver B. It may be caused by Driver B having many behavioral similarities to Driver C and D. This factor is related to the driving geography and the environment, wherein the feature homogenization could reduce the classification performance of the proposed method. Like Driver F, Driver B's data does not participate in the training process so that his driving fragments are assigned to other drivers. Then the DP-based supervisory controller calls a control policy corresponding to the driver for energy distribution to minimize the influence of the defect.

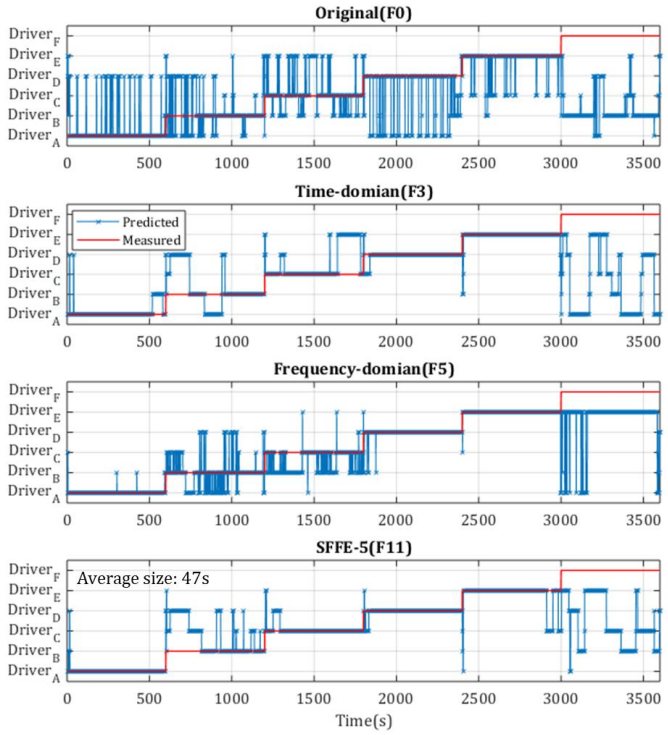

Fig. 8. Real-time performance of driver identification

C. Vehicle Adaptability Performance

This section discusses the fuel economy of the driver-identified control supervisory system and examines vehicle adaptability under different control strategies.

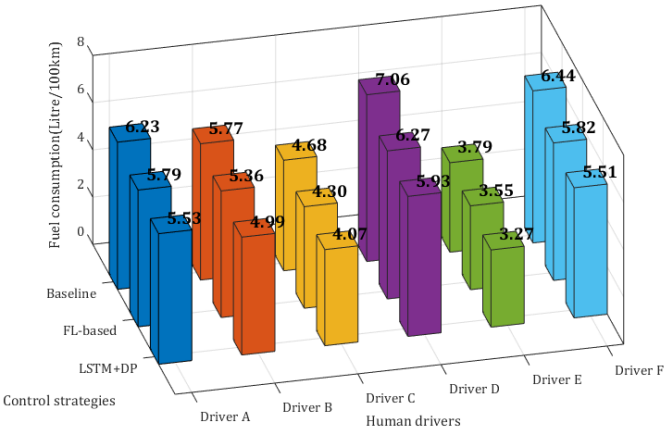

Fig. 9. Fuel consumption comparison over different human drivers

Figure 9 shows fuel consumption comparison over different human drivers, in which each driving cycle in this case is of 60min duration and formed by six 10 min testing fragments from each driver. The data clearly indicates that fuel consumption over different human drivers has significant differences, in which fuel consumption of Driver D (the highest in all testing drivers) is nearly twice that of Driver E. Compared to the baseline and FL-based schemes, the LSTM+DP control strategy always maintains the lowest fuel consumption for all of the drivers. From the perspective of the drivers, the higher the baseline fuel consumption, the greater the energy-saving potential of the LSTM+DP control strategy. Moreover, the gender of human drivers is not considered in the paper but may also affect the energy-saving performance of the developed system, especially, in the way they apply pressure to gas and brake pedals [12].

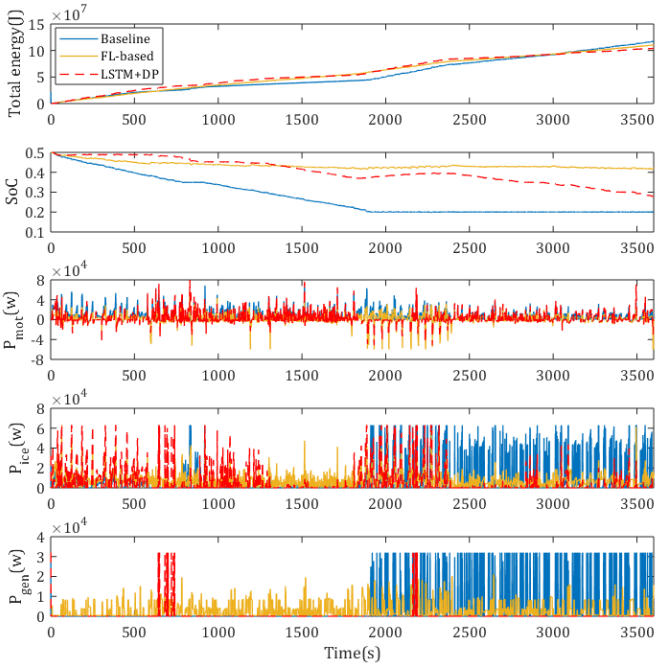

Fig. 10. Real-time performance comparison over different control strategies

In Fig. 10, the driver-identified supervisory control system is further compared with the FL-based (fuzzy logic system) and baseline (charge depleting and charge sustaining control strategy) schemes under real-world driving conditions. These two widely-used strategies considered in the comparison group have both been employed and verified in the author's past work [18], [32]. Differing from FL-based control systems, the SFFE driven system has the unique ability to identify the driver and offer a personalized control policy. The fuel consumption under the proposed control system is significantly lower than other control systems while maintaining relatively higher SoC values. Compared to the baseline control system, both the FL-based and the proposed schemes have stronger robustness in adapting to the driving styles of differing drivers. Differing from the fuzzy control strategy, the DP algorithm considers fuel consumption of HEVs from a global perspective to balance the flow of electricity usage and maximize the fuel economy of HEV systems. The Bi-LSTM helps supervisory control systems to identify target drivers to ensure the effectiveness of

optimized control policies. It is worth mentioning that for Driver F (no knowledge of him in the network), the proposed system has excellent adaptability that continues to operate in the last period (3000 - 3600 s) with the lowest energy consumption. However, the conventional baseline control system has no ability to counter the change of drivers and even driving styles. The vehicle performance with different control strategies is summarized in Table IV. From the results, the LSTM+DP control strategy significantly reduces fuel consumption to 5.2 liter/100 km, and saves 11.31% energy over the baseline (FL-based one saves 5.53%).

TABLE IV
VEHICLE PERFORMANCE COMPARISON OVER REAL-WORLD DRIVING

Control strategy	Final SoC	Fuel consumption (liter/100 km)	Total energy (J)	Energy saving (%)
Baseline	0.2014	6.141	1.1715e+08	-
FL-based	0.4252	5.762	1.1031e+08	5.53%
LSTM+DP	0.2809	5.207	1.0389e+08	11.31%

VI. CONCLUSION

This paper proposes a driver-identified supervisory control system of hybrid electric vehicles (HEVs), wherein an improved method of spectrum-guided fuzzy feature extraction (SFFE) is developed for improving the recognition accuracy and efficiency of this control system. The comparative study including involved extraction methods and their identification system performance as well as its application to HEV systems has been carried out. The contributions drawn from the investigation are as follows:

1) With help of the spectrum-guided fuzzy feature extraction, recognition accuracy of both forward and bi-directional LSTM networks rises 7% and 6% from other extraction methods (time or frequency domain).
2) Compared to forward LSTM networks, bi-directional LSTM networks have a better performance with an average of 7% higher accuracy in driver identification performance.
3) For each human driver, the driver-identified supervisory control system can save more fossil fuel, compared to fuzzy logic-based and rule-based them, especially for driver D (saving up to 16%).
4) Driven by a human driver whose data was not in the training set, this proposed system shows strong robustness and provides excellent energy-saving performance, compared to the baseline (11.31%) and FL-based (5.53%) schemes.

REFERENCES

[1] F. Zhang, X. Hu, R. Langari, and D. Cao, 'Energy management strategies of connected HEVs and PHEVs : Recent progress and outlook', *Progress in Energy and Combustion Science*, vol. 73, pp. 235–256, 2019.

[2] Y. He *et al.*, 'Adaptive Cruise Control Strategies Implemented on Experimental Vehicles: A Review', *IFAC-PapersOnLine*, vol. 52, no. 5, pp. 21–27, 2019.

[3] J. P. F. Trovão, V. D. N. Santos, C. H. Antunes, P. G. Pereirinha, and H. M. Jorge, 'A Real-Time Energy Management Architecture for Multisource Electric Vehicles', *IEEE Transactions on Industrial Electronics*, vol. 62, no. 5, pp. 3223–3233, 2015.

[4] X. Hu, J. Jiang, and S. Member, 'Advanced Power-Source Integration in Hybrid Electric Vehicles : Multicriteria Optimization Approach', *IEEE Transactions on Industrial Electronics*, vol. 62, no. 12, pp. 7847–7858, 2015.

[5] T. Stillwater, K. S. Kurani, and P. L. Mokhtarian, 'The combined effects of driver attitudes and in-vehicle feedback on fuel economy', *Transportation Research Part D*, vol. 52, pp. 277–288, 2017.

[6] X. Qi, P. Wang, G. Wu, S. Member, K. Boriboonsomsin, and M. J. Barth, 'Connected Cooperative Ecodriving System Considering Human Driver Error', *IEEE Transactions on Intelligent Transportation Systems*, vol. 19, no. 8, pp. 2721–2733, 2018.

[7] Y. Huang, H. Wang, A. Khajepour, H. He, and J. Ji, 'Model predictive control power management strategies for HEVs : A review', *Journal of Power Sources*, vol. 341, pp. 91–106, 2017.

[8] Y. Zhou, A. Ravey, and M. Péra, 'Review article A survey on driving prediction techniques for predictive energy management of plug-in hybrid electric vehicles', *Journal of Power Sources*, vol. 412, no. October 2018, pp. 480–495, 2019.

[9] C. M. Martinez, M. Heucke, F. Wang, B. Gao, and D. Cao, 'Driving Style Recognition for Intelligent Vehicle Control and Advanced Driver Assistance : A Survey', *IEEE Transactions on Intelligent Transportation Systems*, vol. 19, no. 3, pp. 666–676, 2018.

[10] P. Ping, W. Qin, Y. Xu, and C. Miyajima, 'Impact of Driver Behavior on Fuel Consumption : Classification , Evaluation and Prediction Using Machine Learning', *IEEE Access*, vol. 7, pp. 78515–78532, 2019.

[11] L. Li, S. You, C. Yang, B. Yan, J. Song, and Z. Chen, 'Driving-behavior-aware stochastic model predictive control for plug-in hybrid electric buses', *Applied Energy*, vol. 162, pp. 868–879, 2016.

[12] A. Wahab, C. Quek, C. K. Tan, and K. Takeda, 'Driving profile modeling and recognition based on soft computing approach', *IEEE Transactions on Neural Networks*, vol. 20, no. 4, pp. 563–582, 2009.

[13] S. Xie, H. He, and J. Peng, 'An energy management strategy based on stochastic model predictive control for plug-in hybrid electric buses', *Applied Energy*, vol. 196, pp. 279–288, 2017.

[14] S. Di Cairano, D. Bernardini, A. Bemporad, and I. V Kolmanovsky, 'Stochastic MPC With Learning for Driver-Predictive Vehicle Control and its Application to HEV Energy Management', vol. 22, no. 3, pp. 1018–1031, 2014.

[15] Y. Zhang *et al.*, 'Optimal energy management strategy for parallel plug-in hybrid electric vehicle based on driving behavior analysis and real time traffic information prediction', *Mechatronics*, vol. 46, pp. 177–192, 2017.

[16] Z. Lei, D. Qin, Y. Liu, Z. Peng, and L. Lu, 'Dynamic energy management for a novel hybrid electric system based on driving pattern recognition', vol. 45, pp. 940–954, 2017.

[17] A. Hossein, G. Jin, X. Yang, and S. Talatahari, 'Chaos-enhanced accelerated particle swarm optimization', *Communications in Nonlinear Science and Numerical Simulation*, vol. 18, no. 2, pp. 327–340, 2013.

[18] J. Li *et al.*, 'Dual-loop online intelligent programming for driver-oriented predict energy management of plug-in hybrid electric vehicles', *Applied Energy*, vol. 253, no. November, p. 113617, 2019.

[19] S. Zhang and R. Xiong, 'Adaptive energy management of a plug-in hybrid electric vehicle based on driving pattern recognition and dynamic programming', *Applied Energy*, vol. 155, pp. 68–78, 2015.

[20] I. V Kolmanovsky, 'Game Theory Controller for Hybrid Electric Vehicles', vol. 22, no. 2, pp. 652–663, 2014.

[21] C. M. Martinez, X. Hu, D. Cao, E. Velenis, B. Gao, and M. Wellers, 'Energy Management in Plug-in Hybrid Electric Vehicles : Recent Progress and a Connected Vehicles Perspective', *IEEE TRANSACTIONS ON VEHICULAR TECHNOLOGY*, vol. 66, no. 6, pp. 4534–4549, 2017.

[22] Q. Zhou *et al.*, 'Multi-step Reinforcement Learning for Model-Free Predictive Energy Management of an Electrified Off-highway Vehicle', *Applied Energy*, vol. 255, no. in press, 2019.

[23] V. Mnih *et al.*, 'Human-level control through deep reinforcement learning', *Nature*, vol. 218, no. 7540, p. 529, 2015.

[24] Y. Wu, H. Tan, J. Peng, H. Zhang, and H. He, 'Deep reinforcement learning of energy management with continuous control strategy and tra ffi c information for a series-parallel plug-in hybrid electric bus', *Applied Energy*, vol. 247, no. March, pp. 454–466, 2019.

[25] M. Sorrentino, V. Cirillo, and L. Nappi, 'Development of flexible procedures for co-optimizing design and control of fuel cell hybrid vehicles', *Energy Conversion and Management*, vol. 185, no. February, pp. 537–551, 2019.

[26] S. Ahmadi, S. M. T. Bathaee, and A. H. Hosseinpour, 'Improving fuel

economy and performance of a fuel-cell hybrid electric vehicle (fuel-cell , battery , and ultra-capacitor) using optimized energy management strategy', *Energy Conversion and Management*, vol. 160, no. December 2017, pp. 74–84, 2018.

[27] A. Kheirandish, F. Motlagh, N. Shafiabady, M. Dahari, A. Khairi, and A. Wahab, 'Dynamic fuzzy cognitive network approach for modelling and control of PEM fuel cell for power electric bicycle system', *Applied Energy*, vol. 202, pp. 20–31, 2017.

[28] E. Kamal, 'Intelligent Energy Management Strategy Based on Artificial Neural Fuzzy for Hybrid Vehicle', *IEEE Transactions on Intelligent Vehicles*, vol. 3, no. 1, pp. 112–125, 2018.

[29] M. Montazeri-gh and M. Mahmoodi-k, 'Optimized predictive energy management of plug-in hybrid electric vehicle based on traffic condition', *Journal of Cleaner Production*, vol. 139, pp. 935–948, 2016.

[30] E. Kamal, 'Hierarchical Energy Optimization Strategy and Its Integrated Reliable Battery Fault Management for Hybrid Hydraulic-Electric Vehicle', *IEEE Transactions on Vehicular Technology*, vol. 67, no. 5, pp. 3740–3754, 2018.

[31] M. Ehsani, Y. Gao, S. Longo, and K. Ebrahimi, *Modern electric, hybrid electric, and fuel cell vehicles*. CRC press, 2018.

[32] J. Li, Q. Zhou, H. Williams, and H. Xu, 'Back-to-back Competitive Learning Mechanism for Fuzzy Logic based Supervisory Control System of Hybrid Electric Vehicles', *IEEE Transactions on Industrial Electronics*, vol. 2, no. c, pp. 1–1, 2019.

[33] Q. Zhou, Y. Zhang, Z. Li, J. Li, H. Xu, and O. Olatunbosun, 'Cyber-Physical Energy-Saving Control for Hybrid Aircraft-Towing Tractor Based on Online', *IEEE TRANSACTIONS ON INDUSTRIAL INFORMATICS*, vol. 14, no. 9, pp. 4149–4158, 2018.

[34] B. C. Miyajima *et al.*, 'Driver Modeling Based on Driving Behavior and Its Evaluation in Driver Identification', 2007.

[35] L. A. H. Zad, 'A fuzzy-algorithmic approach to the definition of complex or imprecise concepts', *International Journal of Man-Machine Studies*, pp. 249–291, 1976.

[36] M. Schuster and K. K. Paliwal, 'Bidirectional Recurrent Neural Networks', vol. 45, no. 11, pp. 2673–2681, 1997.

[37] R. Bellman, 'Dynamic Programming', *Science*, vol. 153, no. 3731, pp. 34–37, 1966.

[38] M. Hessel *et al.*, 'Rainbow: Combining improvements in deep reinforcement learning', *32nd AAAI Conference on Artificial Intelligence, AAAI 2018*, pp. 3215–3222, 2018.

[39] J. S. Wijnands, J. Thompson, G. D. P. A. Aschwanden, and M. Stevenson, 'Identifying behavioural change among drivers using Long Short-Term Memory recurrent neural networks', *Transportation Research Part F: Traffic Psychology and Behaviour*, vol. 53, pp. 34–49, 2018.

Ji Li (M'19) received the B.S. degree (Hons) in vehicle engineering from the Chongqing University of Technology, Chongqing, China, in 2015. He is currently working toward the Ph.D. degree at the Intelligent Vehicle System and Control Team, University of Birmingham, Birmingham, U.K. His current research interests fuzzy mathematics, deep reinforcement learning, Meta-heuristic algorithms and development of man-machine system composed of driving behavior and vehicle intelligent systems.

Quan Zhou (M'17) received the B.Eng. and M.Res. degrees (Hons) in vehicle engineering from Wuhan University of Technology, Wuhan, China, in 2012 and 2015, respectively. He is currently a scholarship-funded Ph.D. Researcher at the Intelligent Vehicle System and Control Team, Vehicle and Engine Technology Research Centre, University of Birmingham, Birmingham, U.K. His research interests include vehicle system modeling, HEV/EV design optimization, optimal control, and artificial intelligence for future HEVs and CAVs.

Yinglong He received the BEng and the MRes degrees in energy and power engineering from Huazhong University of Science and Technology, Wuhan, China, in 2014 and 2017, respectively.

He is currently a scholarship-funded PhD Researcher at the Intelligent Vehicle Control Team, University of Birmingham, Birmingham, UK. His research focuses on emerging vehicular automation and electrification technologies such as adaptive cruise control (ACC), energy management strategy (EMS), and distributed learning and control of the multi-agent system.

Huw Williams is a UK-based business consultant offering a wide range of skills to all types of businesses. He is a professional mathematician with excellent skills in Lean, Six Sigma, Engineering Physics and Statistics. Huw has over 20 years experience in the automotive industry; he graduated from the University of Oxford in 1978 with a mathematics degree and went on to take a PhD in theoretical mechanics at the University of East Anglia. His early career comprised research work on the mechanical properties of ice for the US Army followed by a spell as a mathematics lecturer at Edinburgh's Heriot-Watt University where he researched in theoretical mechanics. Huw joined Jaguar Cars in 1986 where he worked in research and development applying mathematical modelling techniques to all aspects of vehicle technology. He also developed statistical skills through TQM in the 1980's culminating in his accreditation as Ford's top-scoring Master Black Belt in 2005.

Hongming Xu received the Ph.D. degree in mechanical engineering from Imperial College London, London, U.K. He is a Professor of Energy and Automotive Engineering at the University of Birmingham, Birmingham, U.K., and the Head of Vehicle and Engine Technology Research Centre. He has six years of industrial experience with Jaguar Land Rover and Premier Automotive Group of Ford. He has authored and co-authored more than 300 journal and conference publications on advanced vehicle powertrain systems involving both experimental and modeling studies.

Prof. Xu was a member of the Ford HCCI Global Steering Committee, a Project Manager and Technical Leader of U.K. Foresight Vehicle LINK projects CHARGE and CHASE from 2002 to 2007. He is a Fellow of SAE International and IMechE.